ISSN 1063-7761, Journal of Experimental and Theoretical Physics, 2016, Vol. 122, No. 5, pp. 859–868. © Pleiades Publishing, Inc., 2016.
Original Russian Text © R.M. Khusnutdinoff, A.V. Mokshin, S.G. Menshikova, A.L. Beltyukov, V.I. Ladyanov, 2016, published in Zhurnal Eksperimental'noi i Teoreticheskoi Fiziki, 2016, Vol. 149, No. 5, pp. 994–1004.

SOLIDS AND LIQUIDS

Viscous and Acoustic Properties of AlCu Melts

R. M. Khusnutdinoff[a, b]*, A. V. Mokshin[a, b], S. G. Menshikova[c], A. L. Beltyukov[c], and V. I. Ladyanov[c]**

[a] *Kazan Federal University, Kazan, 420008 Russia*
[b] *Landau Institute of Theoretical Physics, Russian Academy of Sciences, Chernogolovka, Moscow oblast, 142432 Russia*
[c] *Physicotechnical Institute, Ural Branch, Russian Academy of Sciences, Izhevsk, 426000 Russia*
**e-mail: khrm@mail.ru; **e-mail: anatolii.mokshin@mail.ru*

Received September 26, 2015

Abstract—The atomic dynamics of the binary $Al_{100-x}Cu_x$ system is simulated at a temperature $T = 973$ K, a pressure $p = 1.0$ bar, and various copper concentrations x. These conditions (temperature, pressure) make it possible to cover the equilibrium liquid $Al_{100-x}Cu_x$ phase at copper concentrations $0 \leqslant x \leqslant 40\%$ and the supercooled melt in the concentration range $40\% \leqslant x \leqslant 100\%$. The calculated spectral densities of the time correlation functions of the longitudinal $\tilde{C}_L(k, \omega)$ and transverse $\tilde{C}_T(k, \omega)$ currents in the $Al_{100-x}Cu_x$ melt at a temperature $T = 973$ K reveal propagating collective excitations of longitudinal and transverse polarizations in a wide wavenumber range. It is shown that the maximum sound velocity in the $v_L(x)$ concentration dependence takes place for the equilibrium melt at an atomic copper concentration $x = 10 \pm 5\%$, whereas the supercooled $Al_{100-x}Cu_x$ melt saturated with copper atoms ($x \geqslant 40\%$) is characterized by the minimum sound velocity. In the case of the supercooled melt, the concentration dependence of the kinematic viscosity $\nu(x)$ is found to be interpolated by a linear dependence, and a deviation from the linear dependence is observed in the case of equilibrium melt at $x < 40\%$. An insignificant shoulder in the $\nu(x)$ dependence is observed at low copper concentrations ($x < 20\%$), and it is supported by the experimental data. This shoulder is caused by the specific features in the concentration dependence of the density $\rho(x)$.

DOI: 10.1134/S1063776116040166

1. INTRODUCTION

Owing to their unique physicochemical properties, aluminum-containing copper alloys (copper-based duralumins and aluminum alloys–aluminum bronzes) are widely used in mechanical engineering and aircraft industry [1]. For example, apart from a small weight and a high strength, aluminum–copper alloys are characterized by a high plasticity and a high corrosion resistance. Their physical properties (thermal conductivity, viscosity, electrical resistivity, magnetic susceptibility, etc.) are mainly determined by the ratio of the concentrations of their components, namely, Al and Cu atoms [2–5].

A binary $Al_{100-x}Cu_x$ aluminum alloy is characterized by a complex phase diagram, which has a melt at temperatures $T \geqslant 820$ K (at a pressure $p = 1.0$ bar and a copper concentration $x \approx 17.5\%$) and an extended field containing various crystalline phases (see the phase diagram of the $Al_{100-x}Cu_x$ melt in Fig. 1). As was shown in [5–7], aluminum-containing alloys have a high glass-forming ability. Viscosity is one of the most important characteristics that determine the glass-forming ability of a substance [8]. For example, the authors of [9] used experimental data for the temperature dependence of the viscosity of the supercooled $Al_{80}Cu_{20}$ melt and found maximum viscosities at $T = 1053$ and 1123 K. On the other hand, the presence of extrema in viscosity isotherms in the aluminum–copper Cu_3Al melt was noted in [10, 11]. The appearance of these features was assumed to be related to the existence of "quasicrystalline microgroups" in the liquid phase.

The concentration dependence of shear viscosity $\eta(x)$ of the $Al_{100-x}Cu_x$ melt at a temperature $T = 1500$ K was experimentally studied in [12]. The maximum viscosity was detected in the $T = 1500$ K isotherm at a copper concentration $x \approx 70\%$. This specific feature in the $\eta(x)$ dependence was explained in terms of a phenomenological theory, which takes into account the enthalpy of mixing ΔH_{mix}, the viscosity, and the activation energy of pure Al and Cu melts. The isotherms of kinematic viscosity ν of the $Cu_{100-x}Al_x$ melt were investigated in the wide temperature range between liquidus and $T = 1723$ K. The $\nu(x)$ concentration dependences exhibited maxima near the stoichiometric $CuAl_3$ concentration and the $Al_{30}Cu_{70}$ composition and the branching of the temperature dependences of kinematic viscosity $\nu(T)$ obtained upon

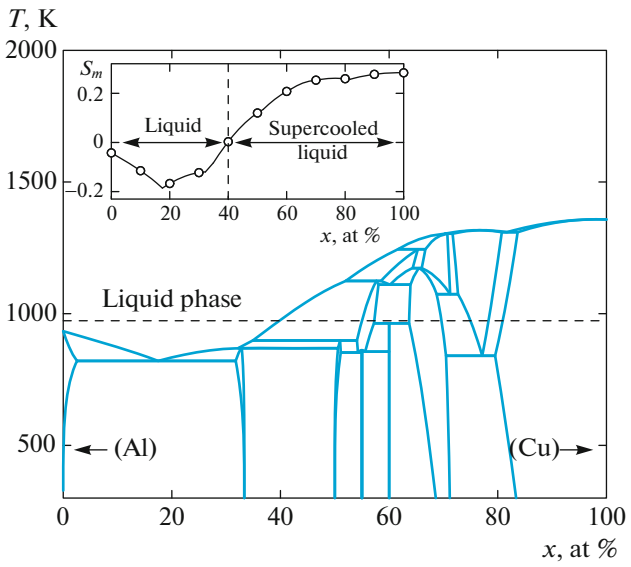

Fig. 1. (Color online) Aluminum–copper $Al_{100-x}Cu_x$ phase diagram [15, 16]. (dashed line) Isotherm–isobar ($T = 973$ K, $p = 1.0$ bar) in which the system is considered. (inset) Parameter $S_m = (T_m - T)/T_m$ vs. atomic copper concentration x.

heating and subsequent cooling, the so-called viscosity hysteresis.

Thus, conflicting experimental data on the specific features of the viscosity of the AlCu melts have been collected to date, and the mechanisms that cause these specific features are poorly understood. The purpose of this work is to simulate the atomic dynamics of the binary $Al_{100-x}Cu_x$ system at various copper concentrations x, a temperature $T = 973$ K, and a pressure $p =$ 1.0 bar. The corresponding isotherm–isobar is represented by the dashed line in Fig. 1. The inset to Fig. 1 shows parameter $S_m = (T_m - T)/T_m$ versus atomic copper concentration x in the $Al_{100-x}Cu_x$ system. Dimensionless parameter S_m characterizes the relative distance of the state of the system from the state of melting at temperature T_m. For example, we have $S_m = 0$ at melting temperature T_m. In the case of equilibrium melt at temperatures higher than melting temperature T_m, we have $S_m < 0$, whereas this parameter takes positive values ($S_m > 0$) at $T < T_m$. In the case of a supercooled liquid (melt) at $T < T_m$, this parameter is identical to a well-known quantity, namely, the level of supercooling [14].

We consider equilibrium melts for the chosen states at $T = 973$ K, $p = 1.0$ bar, and copper concentrations $x < 40\%$. As is seen from the phase diagram shown in Fig. 1, the equilibrium states of the system are related to crystalline phases at copper concentrations $x \geqslant 40\%$ and the given temperature and pressure. Therefore, we consider samples corresponding to supercooled melts for this concentration range ($x \geqslant 40\%$). For this concentration range, we calculate the viscosity and the spectral densities of the time correlation functions of longitudinal and transverse currents at various wavenumbers.

2. SIMULATION PROCEDURE

The atomic dynamics of the metallic $Al_{100-x}Cu_x$ melt was simulated at a temperature $T = 973$ K and an external pressure $p = 1.0$ bar. The system under study consists of $N = 4000$ atoms located in a cubic cell with periodic boundary conditions. Interatomic interaction was performed via the embedded-atom method (EAM) potential developed specifically for the binary AlCu melt [17].[1] According to [17], the potential energy of the i-th atom in the AlCu melt can be expressed as

$$U_i = F_\alpha\left(\sum_{j\neq 1}\rho_\beta(r_{ij})\right) + \frac{1}{2}\sum_{j\neq 1}\phi_{\alpha\beta}(r_{ij}), \qquad (1)$$

where $\phi_{\alpha\beta}(r_{ij})$ is the short-range order pair potential of interatomic interaction and $F(\rho)$ is the embedded-atom potential, which takes into account multiparticle interactions through so-called "effective" electron density ρ_i of the ith atom. Subscripts α and β indicate the types of the elements that enter into the composition of the metallic alloy, $\alpha, \beta \in \{Al,Cu\}$.

The $Al_{100-x}Cu_x$ system was formed by rapid cooling of the equilibrium melt with temperature $T = 3000$ K. The cooling rate of the system was $dT/dt = 10^{12}$ K/s. The equation of atom motion was integrated using the Verlet algorithm in the velocity form at a time step $\delta t =$ 1.0 fs [18, 19]. To bring the system to the state of thermodynamic equilibrium, a program performed 4.5×10^6 time steps in an NpT ensemble and 5×10^6 steps in an NVT ensemble to calculate time and spectral characteristics.

3. EXPERIMENTAL

Kinematic viscosity ν of the melts was measured using torsional vibrations on a computer-assisted device [20]. The measurements were performed in cylindrical Al_2O_3 crucibles with a cover at the upper melt boundary (inside a crucible) in a protective helium atmosphere. During measurements, the cover played the role of the second face surface of friction [21]. The temperature dependences of viscosity were obtained upon heating and subsequent cooling. Before measurements, isothermal holding for 10 min was carried out at each temperature. The melt temperature was determined accurate to ±5 K with a tungsten–rhenium thermocouple, which was placed under the bottom of the crucible. The thermocouple readings

[1] This potential model can be applied to metals Al, Ag, Au, Cu, Ni, Pd, and Pt and binary melts.

were calibrated against the melting temperatures of pure metals (Al, Cu, Ni, Co, Fe).

When calculating viscosity, we solved the following equation using numerical methods [20, 22]:

$$f(\nu) = \mathrm{Re}\,\mathcal{L} + \frac{\delta}{2\pi}\mathrm{Im}\,\mathcal{L} - 2I\left(\frac{\delta}{\tau} - \frac{\delta_0}{\tau_0}\right) = 0, \qquad (2)$$

where I is the moment of inertia of the suspension system and δ and τ (δ_0, τ_0) are the damping constant and the vibration period of the suspension system with the melt (without the melt), respectively. $\mathrm{Re}\,\mathcal{L}$ and $\mathrm{Im}\,\mathcal{L}$ are the real and imaginary parts of the friction function, which take into account the existence of two face frictional surfaces.

To calculate the error of measuring the viscosity, we used the method described in detail in [23]. The total relative error of determining the viscosity did not exceed 4% at an error of 2% in an individual experiment.

4. SIMULATION RESULTS

4.1. Structural Features of the $Al_{100-x}Cu_x$ Melt

The structural features of the $Al_{100-x}Cu_x$ melt can be analyzed using the atomic radial distribution function (RDF) [24]

$$g(r) = \sum_{\alpha=\beta} W_{\alpha,\beta} g_{\alpha,\beta}(r) + 2\sum_{\alpha\neq\beta} W_{\alpha,\beta} g_{\alpha,\beta}(r), \qquad (3)$$

where $W_{\alpha,\beta} = c_\alpha c_\beta f_\alpha f_\beta / (\sum c_i f_i)^2$ is the weight factor and c_i and f_i are the concentration and the form factor of atoms of the i-th kind. The partial components of RDF $g_{\alpha,\beta}(r)$ were determined from the expression [25, 26]

$$g_{\alpha,\beta}(r) = \frac{L^3}{N_\alpha N_\beta}\left\langle \sum_{j=1}^{N_\alpha} \frac{n_{j\beta}(r)}{4\pi r^2 \Delta r} \right\rangle, \quad a,\beta \in \{\mathrm{Al},\mathrm{Cu}\}, \qquad (4)$$

where $n_{j\beta}(r)$ is the number of atoms of kind β in the spherical layer of thickness Δr located at distance r from the j-th particle; L is the edge length of the cell to be simulated; and N_α and N_β are the numbers of atoms of kinds α and β, respectively.

Figure 2 shows RDF $g(r)$ and static structure factor $S(k)$, which were calculated by simulating the atomic dynamics of pure liquid Al and Cu at a temperature $T = 1323$ and 1423 K, respectively. Here, the calculation results are compared with the experimental data obtained by X-ray diffraction [27]. The simulation results are seen to agree well with the experimental data: the structural features of the pure copper and aluminum melts are correctly reproduced.

Figure 3 shows RDF $g(r)$ for the $Al_{100-x}Cu_x$ melt at a temperature $T = 973$ K and the translational order parameter [28, 29]

$$t = \frac{1}{r_m}\int_0^{r_m} |g(r) - 1| dr \qquad (5)$$

at various atomic copper concentration x. In Eq. (5), quantity r_m is the distance at which the correlation of two particles becomes insignificant. In this work, we have $r_m = 20$ Å. Note that the translational order parameter is $t \to 0$ for random systems and $t \to 1$ for crystalline bodies. It is seen from Fig. 3a that, as the atomic copper concentration changes in the $Al_{100-x}Cu_x$ system, no substantial changes in the structure of the melt is observed. The calculated concentration dependence of the translational order parameter indicates that parameter $t(x)$ changes in the range $0.184 \leqslant t \leqslant 0.192$ in the case of equilibrium melt (at copper concentrations $0 \leqslant x \leqslant 40\%$) and increases linearly from $t(x = 40\%) = 0.192$ to $t(x = 100\%) = 0.228$ for the supercooled melt with a copper concentration $40\% \leqslant x \leqslant 100\%$. It is interesting that the character of the dependence changes at a concentration $x = 40\%$, which corresponds to the boundary between the equilibrium liquid and the supercooled liquid in the given isotherm–isobar (see Fig. 1). Note that the linear character of the concentration dependence of parameter $t(x)$ in the concentration range $40\% \leqslant x \leqslant 100\%$ is analogous to the temperature dependence of this parameter for the corresponding supercooled liquids [28].

4.2. Microscopic Dynamics of the Metallic $Al_{100-x}Cu_x$ Melt

The collective dynamics of particles in the metallic $Al_{100-x}Cu_x$ melt was analyzed by calculating the spectral densities

$$\tilde{C}_\alpha(k,\omega) = \frac{k_B T}{\pi m}\int_0^\infty C_\alpha(k,t) e^{i\omega t} dt, \quad \alpha \in \{L,T\} \qquad (6)$$

and the normalized time correlation functions (TCFs) of the longitudinal current

$$C_L(k,t)\frac{\langle (\mathbf{e}_k \cdot \mathbf{j}_k^*(0) \cdot \mathbf{e}_k \cdot \mathbf{j}_k(t))\rangle}{\langle |\mathbf{e}_k \cdot \mathbf{j}_k(0)|^2\rangle}, \qquad (7)$$

and the transverse current [30, 31]

$$C_T(k,t)\frac{\langle [\mathbf{e}_k \times \mathbf{j}_k^*(0)] \cdot [\mathbf{e}_k \times \mathbf{j}_k(t)]\rangle}{\langle |[\mathbf{e}_k \times \mathbf{j}_k(0)]|^2\rangle}. \qquad (8)$$

Here, $\mathbf{j}(k, t)$ is the microscopic current determined by the expression [25, 32]

$$\mathbf{j}(k,t) = \frac{1}{\sqrt{N}}\sum_l^N \mathbf{v}_l(t)\exp[-i(\mathbf{k}\cdot\mathbf{r}_l(t))], \qquad (9)$$

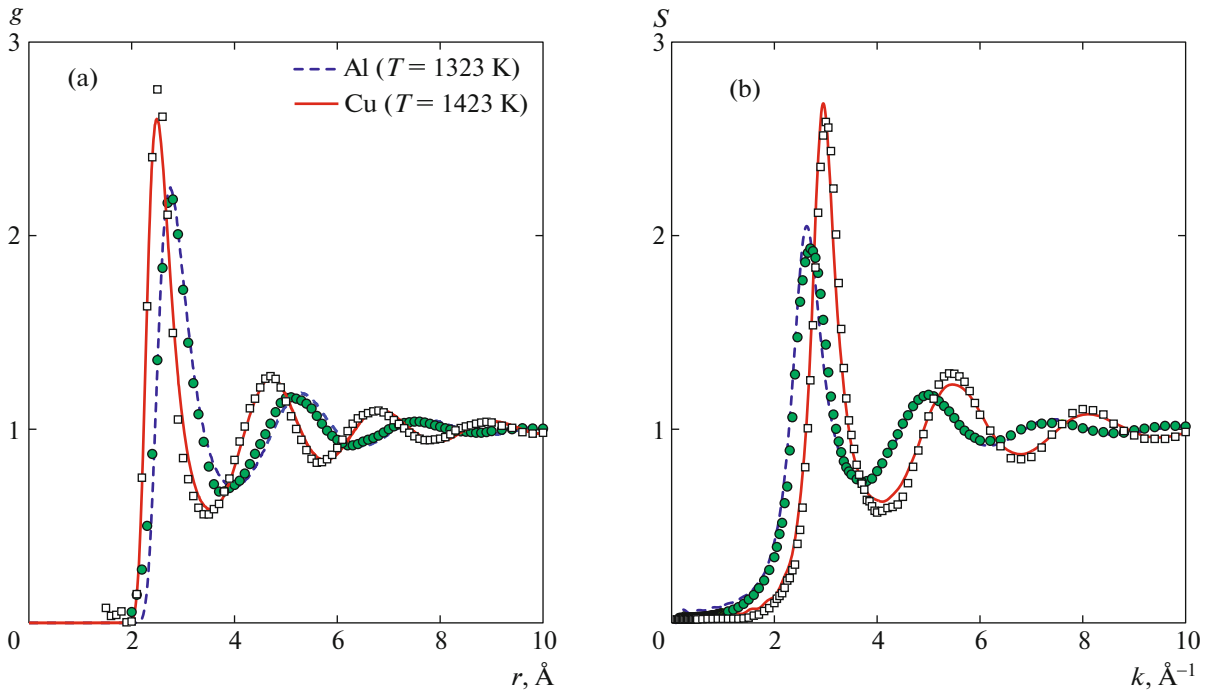

Fig. 2. (Color online) (a) RDF of aluminum and copper atoms in the melt at a temperature $T = 1323$ and 1423 K, respectively: (solid and dashed curves) results of atomic dynamics simulation and (symbols) X-ray diffraction data [27]. (b) Static structure factor of the aluminum and copper melts.

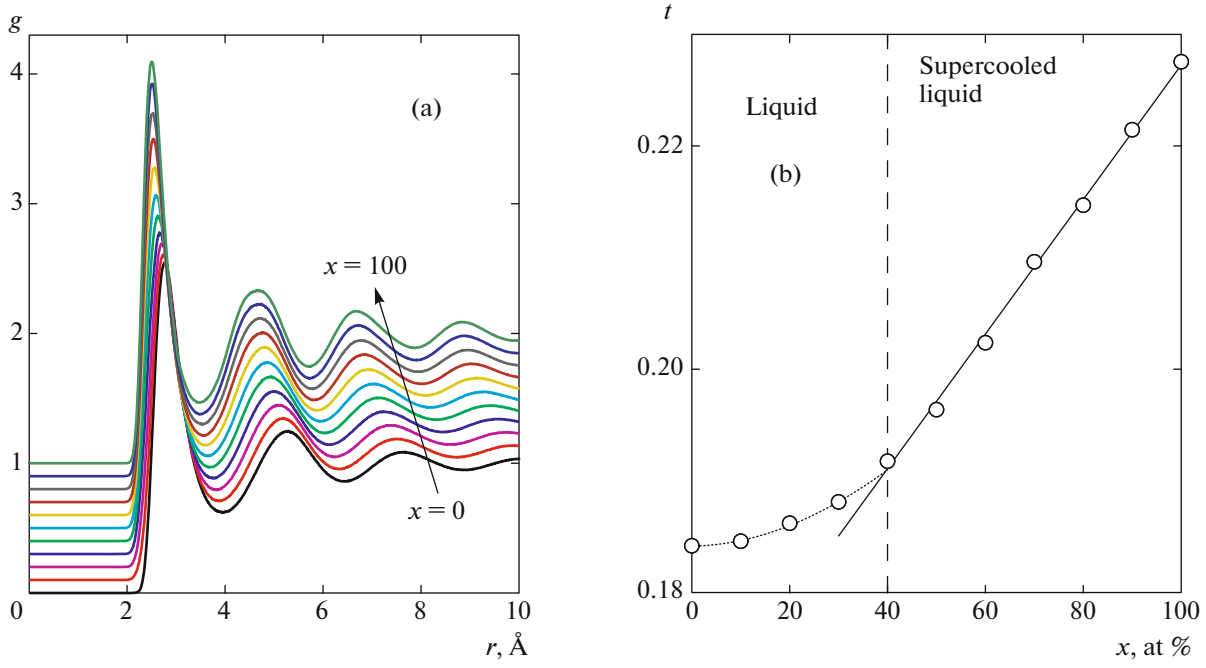

Fig. 3. (Color online) (a) RDF of atoms in the $Al_{100-x}Cu_x$ melt at $T = 973$ K. (b) Translational order parameter t vs. the atomic copper concentration.

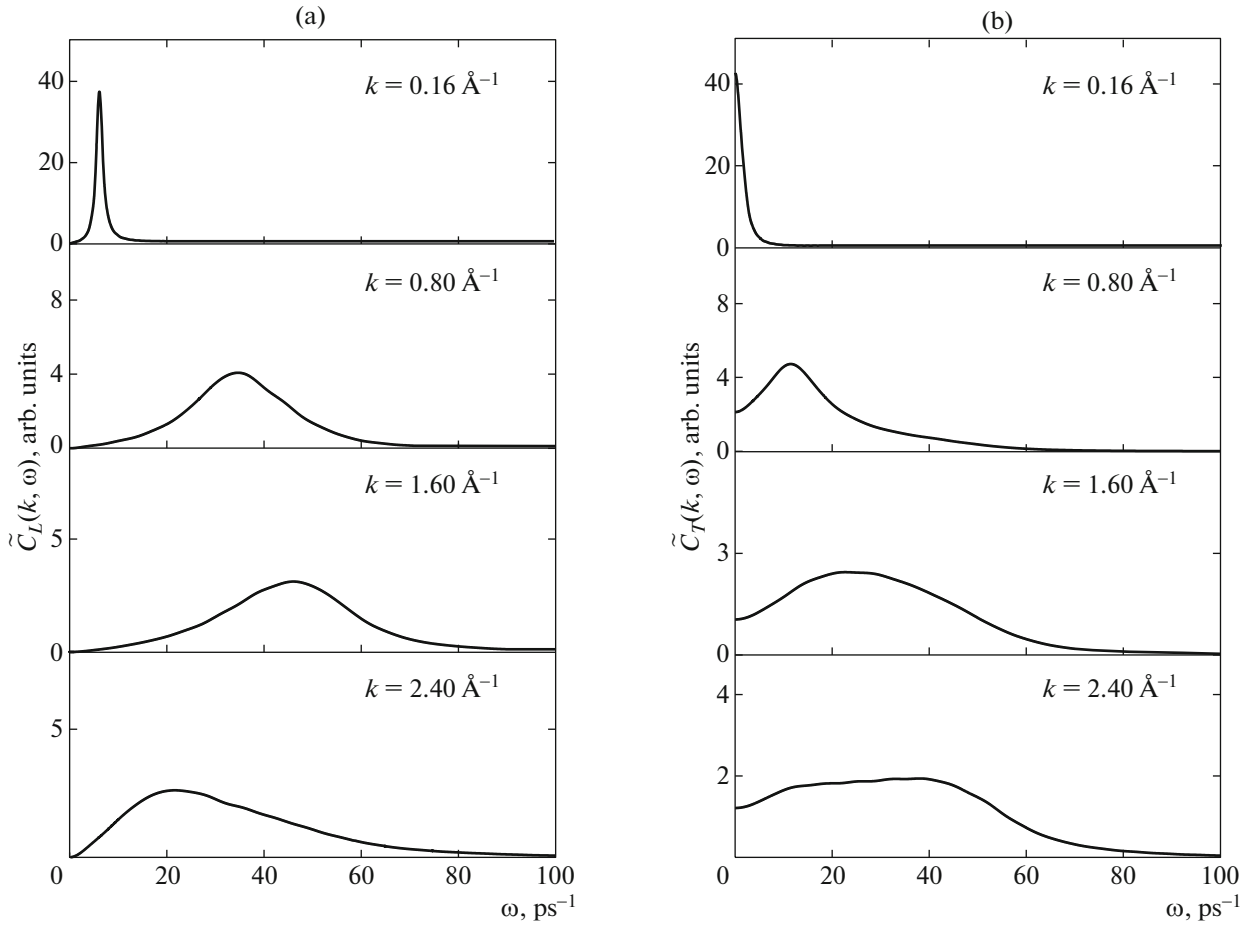

Fig. 4. Spectral densities of TCFs of (a) longitudinal $\tilde{C}_L(k,\omega)$ and (b) transverse $\tilde{C}_T(k,\omega)$ currents of the $Al_{50}Cu_{50}$ melt at $T =$ 973 K.

where $\mathbf{v}_l(t)$ is the velocity of the l-th particle at time t and $\mathbf{e}_k = \mathbf{k}/|\mathbf{k}|$ is the unit vector codirectional with wavevector $\mathbf{k}$.

To remove noises from the spectral densities of the TCFs of the longitudinal and transverse currents, we applied "window" averaging with the Gaussian function [29]

$$\tilde{C}_\alpha^{av}(k,\omega) = \int_{-\infty}^{\infty} R(\omega-\omega')\tilde{C}_\alpha(k,\omega')d\omega', \quad a \in \{L,T\}, \tag{10}$$

where the resolution function

$$R(\omega) = \frac{1}{\sqrt{\pi}\omega_0}\exp\left(-\frac{\omega^2}{\omega_0^2}\right) \tag{11}$$

satisfies the normalization condition

$$\int_{-\infty}^{\infty} R(\omega)d\omega = 1. \tag{12}$$

Frequency ω_0 was determined by the time scale of simulation and was found to be $\omega_0 = 2\pi/N\delta t \approx 1.2$ ns^{-1}.

Figure 4 shows the spectral densities of TCFs $\tilde{C}_L(k,\omega)$ and $\tilde{C}_T(k,\omega)$ for the supercooled $Al_{50}Cu_{50}$ melt at a temperature $T = 973$ K for a wide wavevector range $k = 0.16$–2.40 Å^{-1}. Both spectral characteristics $\tilde{C}_L(k,\omega)$ and $\tilde{C}_T(k,\omega)$ have pronounced high-frequency peaks, which point to the existence of collective vibrational processes in the melt. Although the $\tilde{C}_L(k,\omega)$ and $\tilde{C}_T(k,\omega)$ spectra have a similar shape, the characters of their vibrational spectra are substantially different.

When calculating the spectral densities of TCFs of the longitudinal $\tilde{C}_L(k,\omega)$ and transverse $\tilde{C}_T(k,\omega)$ currents, we were able to estimate the dispersion $\omega_c^{(\alpha)}(k)$ dependences (see Fig. 5). In the case of the supercooled $Al_{50}Cu_{50}$ melt, we detected vibrational modes of longitudinal and transverse polarizations. The dispersion curve related to the vibrational processes of transverse polarization is characterized by a window of

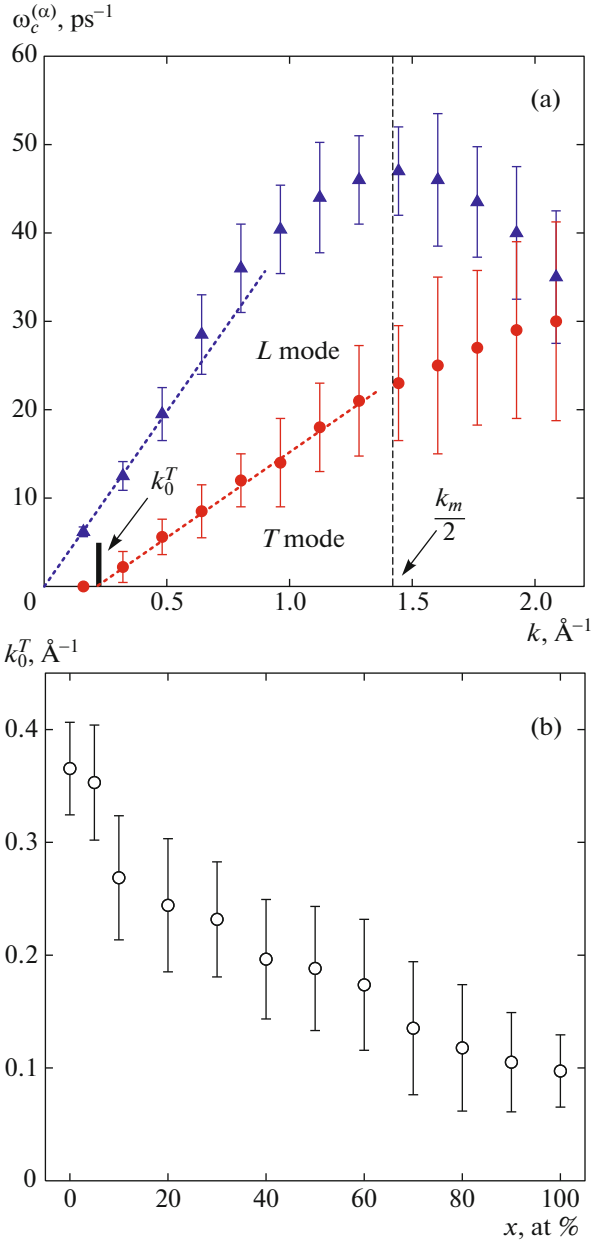

Fig. 5. (Color online) (a) Dispersion curves for the Al_{50}-Cu_{50} melt vs. wavenumber k at $T = 973$ K: (dotted lines) extrapolated hydrodynamic result $\omega_c^{(\alpha)}(k) = v_\alpha(k - k_0^\alpha)$, where v_α is the velocity of longitudinal ($\alpha \equiv L$) and transverse ($\alpha \equiv T$) polarization sound and k_0^α is wavenumber k at which $\omega(k)$ begins to be nonzero. Here, we have $k_0^L = 0$ Å^{-1} for the longitudinal mode and $k_0^T = 0.188$ Å^{-1} for the transverse mode. (dashed line) Boundary of the first Brillouin pseudozone at $k_m/2$, where k_m is the position of the principal maximum in static structure factor $S(k)$. (b) Concentration dependence of gap width $k_0^T(x)$ in the dispersion curve of transverse polarization $\omega_c^{(T)}(k)$.

width k_0^T: $\omega_c^{(T)}(k)$ is shifted by k_0^T along axis k rather than beginning from a zero value. The presence of $k_0^T \neq 0$ is caused by the absence of macroelastic properties of the melt (both equilibrium and supercooled melts) [33]. The window width was found to decrease with increasing copper concentration in the melt. For example, we have $k_0^T = 0.37$ Å^{-1} for the pure aluminum melt and $k_0^T = 0.097$ Å^{-1} for the pure supercooled copper melt. It is interesting that the concentration dependence of k_0^T decreases gradually and has no specific features at an intermediate concentration $x = 40\%$.

The collective dynamics of melt atoms is characterized by the following frequency moments of the spectral dependences of the TCFs of the longitudinal $\tilde{C}_L(k,\omega)$ and transverse $\tilde{C}_T(k,\omega)$ currents [34]:

$$\omega_\alpha^{(2n)}(k) = \int_{-\infty}^{\infty} \omega^{2n}\tilde{C}_\alpha(k,\omega)d\omega \Big/ \int_{-\infty}^{\infty} \tilde{C}_\alpha(k,\omega)d\omega = (-1)^n \left(\frac{d^{(2n)}C_\alpha(k,t)}{dt^{(2n)}}\right)\Bigg|_{t=0}, \quad n = 1, 2, \ldots. \tag{13}$$

Only the even moments become nonzero. For example, the second moments of the $\tilde{C}_L(k,\omega)$ and $\tilde{C}_T(k,\omega)$ spectral densities in the case of a spherical pair potential of interparticle interaction $U(r)$ can be determined from the following microscopic expressions [35, 36]:

$$\omega_L^2(k) = 3v_{\text{th}}^2k^2 + \frac{n}{m}\int_0^\infty g(r)[1-\cos(kz)] \times \frac{\partial^2 U(r)}{\partial x^2}d^3r. \tag{14}$$

$$\omega_T^2(k) = 3v_{\text{th}}^2k^2 + \frac{n}{m}\int_0^\infty g(r)[1-\cos(kz)] \times \frac{\partial^2 U(r)}{\partial x^2}d^3r, \tag{15}$$

where $v_{\text{th}} = \sqrt{k_B T/m}$ is the thermal velocity of particles, $n = N/V$ is the numerical density of the system, and $g(r)$ is the total RDF of two particles. Figure 6 shows the results of simulation of the frequency moments of the spectral densities of TCFs of the longitudinal and transverse currents for a wide wavenumber range that were calculated by Eq. (13). It is seen that the frequency moments of the spectral dependences of the TCFs of the longitudinal $\tilde{C}_L(k,\omega)$ and transverse $\tilde{C}_T(k,\omega)$ currents, $\omega_L(k)$ and $\omega_T(k)$, have a k dependence, which is similar to the $\omega_c^{(L)}(k)$ and $\omega_c^{(T)}(k)$ dispersion curves. Note that the positions of

the maxima in the $\omega_L^2(k)$ and $\omega_T^2(k)$ curves correspond exactly to the positions of the peaks in the $\omega_c^{(L)}(k)$ and $\omega_c^{(T)}(k)$ curves.

Using the dispersion curves, we calculated the concentration dependences of the sound velocities of longitudinal and transverse polarizations. Figure 7 shows the longitudinal (v_L) and transverse (v_T) polarization sound velocities in the $Al_{100-x}Cu_x$ system at various atomic copper concentrations. $v_L(x)$ increases at a low copper concentration. At an atomic copper concentration $x = 10 \pm 5\%$, sound velocity v_L reaches its maximum ($v_L \approx 4.7$ km/s). Then, it decreases when concentration c increases. The decrease of v_L almost terminates at a concentration $x = 40\%$, which corresponds to the transition of the equilibrium melt into the supercooled melt. Thus, the sound velocity in the concentration dependence $v_L(x)$ is maximal for the equilibrium melt, and the supercooled $Al_{100-x}Cu_x$ melt saturated with copper atoms is characterized by the minimum sound velocity ($v_L \approx 3.94$ km/s). Note that the character of the $v_L(x)$ dependence correlates with the concentration dependence of parameter $S_m(x)$, which characterizes the distance of the system from melting temperature T_m. Thus, the maximum sound velocity v_L corresponds to the state of equilibrium melt, which is distant from the melting temperature as far as possible.

As the copper concentration increases, the velocity of transverse polarization sound $v_T(x)$ decreases from $v_T = 2.74$ km/s to 1.79 km/s. The ratios of the sound velocities of longitudinal and transverse polarizations for the aluminum melt ($x = 0\%$) and the supercooled copper melt ($x = 100\%$) at a temperature $T = 973$ K were found to be $v_L/v_T = 1.67$ and 2.19, respectively.

Based on the data of simulation of the atomic dynamics from the normalized TCF of transverse current $C_T(k, t)$, we calculated the shear viscosity [37]

$$\eta_s(k) = \rho\left(k^2\int_0^\infty C_T(k,t)dt\right)^{-1} \quad (16)$$

and the kinematic viscosity [38, 39]

$$\nu = \eta_s/\rho. \quad (17)$$

Here, ρ is the mass density of the system. Figure 8 shows the results of simulation of the shear $\eta(k)$ and kinematic $\nu(k)$ viscosities as functions of wavenumber k at various atomic copper concentrations. To extrapolate the simulation results, we used the function [40]

$$\eta_s(k) = \frac{\eta_0}{1+\alpha^2k^2}, \quad (18)$$

with fitting parameters α and η_0.

Based on the results of simulation of the atomic dynamics, we also calculated the concentration dependences of the coefficients of shear $\eta_s(x)$ and kinematic $\nu(x)$ viscosities. Figure 9 depicts the obtained results in comparison with the experimental data. The simulation results are seen to correctly reproduce the experimental data on the kinematic viscosity of the $Al_{100-x}Cu_x$ melt at a temperature $T = 973$ K for the atomic copper concentration range from $x > 0\%$ to $x = 30\%$. Moreover, the simulation and experimental results indicate that an increase in the atomic copper concentration in the melt leads to an increase in the viscosity. As the copper concentration increases, the kinematic viscosity increases from $\nu = 4.2 \times 10^{-7}$ to 9.3×10^{-7} m^2/s. Note that the total concentration dependence is characterized by two modes. In the case of the supercooled melt saturated with cop-

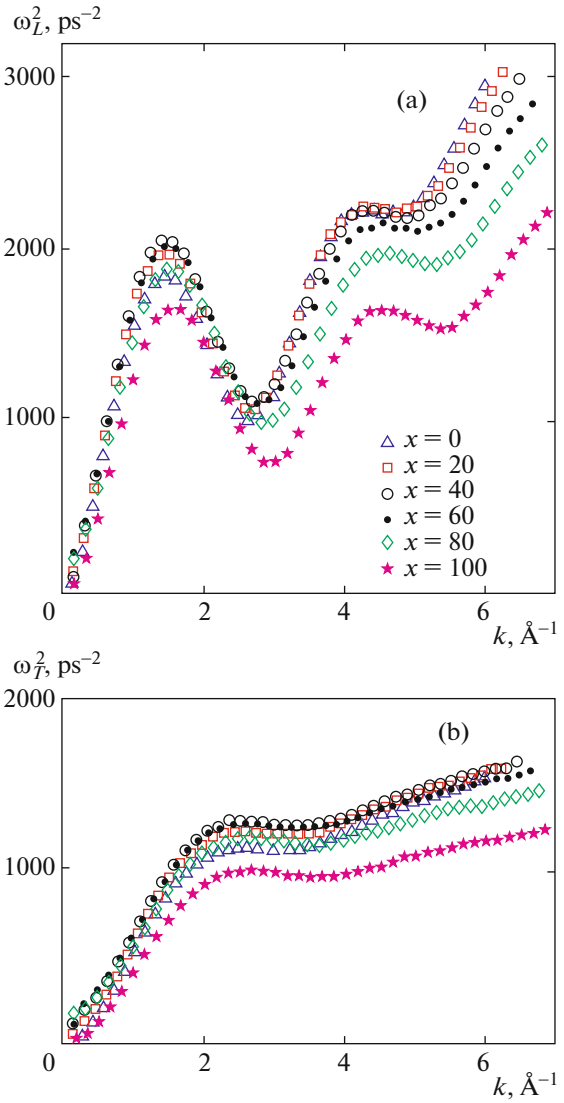

Fig. 6. (Color online) Normalized frequency moments of the spectral densities of TCFs of (a) longitudinal and (b) transverse flows for the metallic $Al_{100-x}Cu_x$ melt vs. wavenumber k at various atomic copper concentrations.

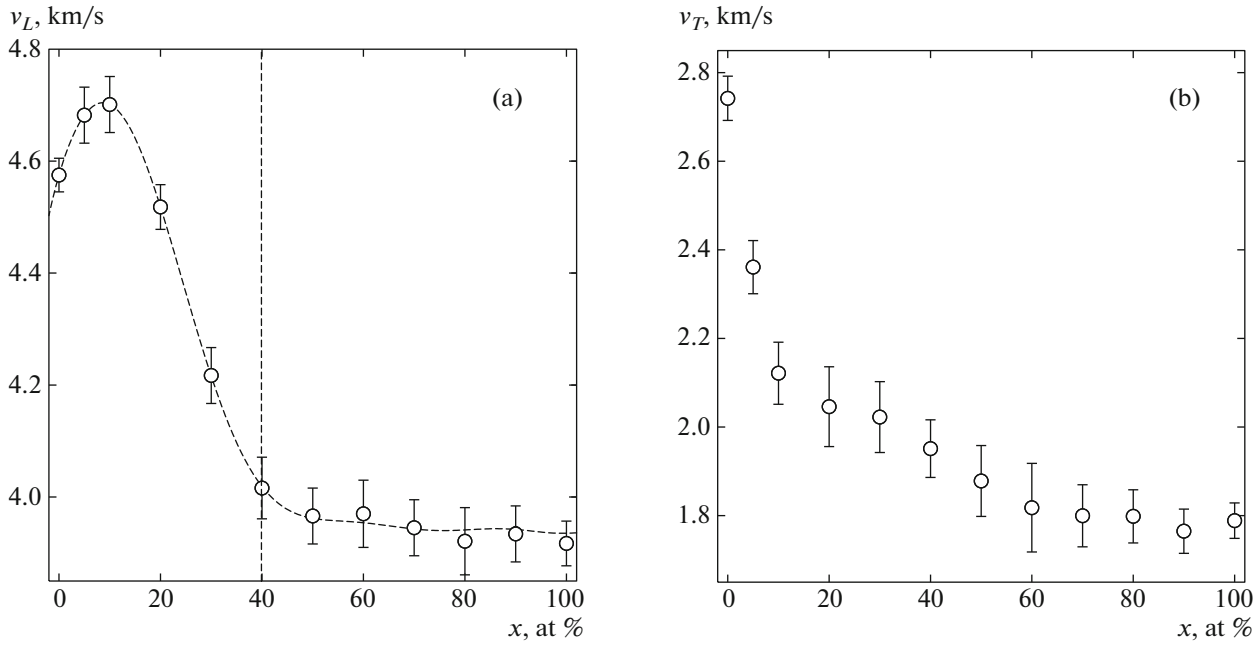

Fig. 7. Velocities of (a) longitudinal and (b) transverse polarization sound in the metallic $Al_{100-x}Cu_x$ melt vs. the atomic copper concentration at $T = 973$ K.

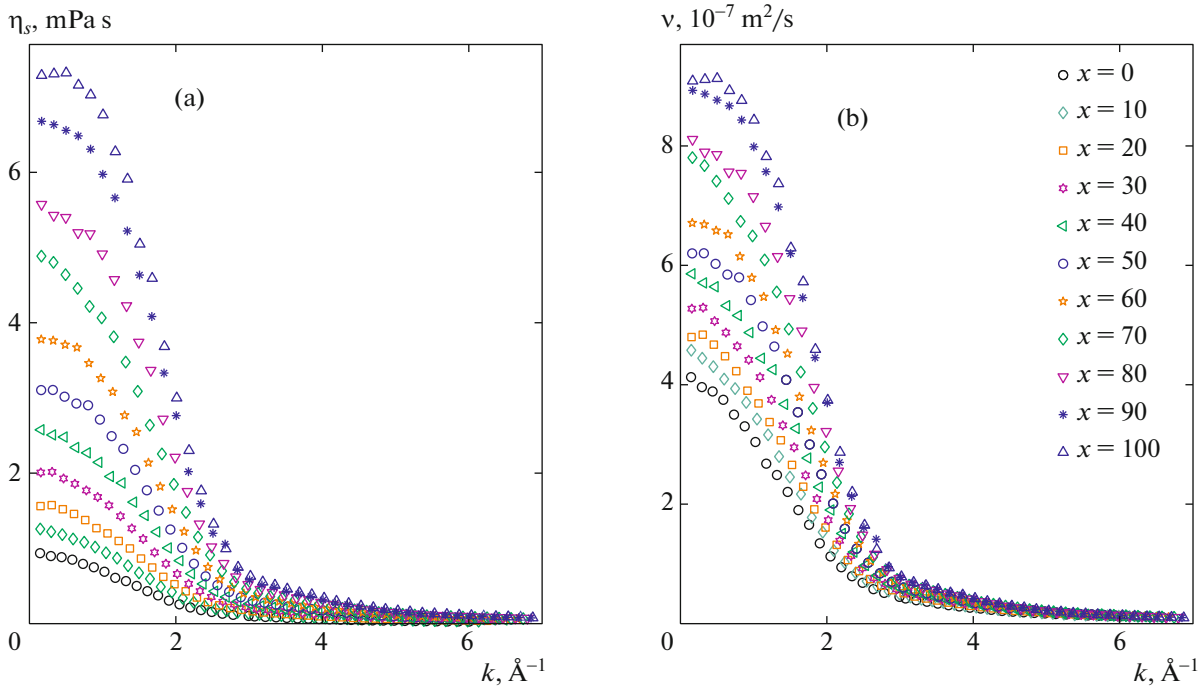

Fig. 8. (Color online) (a) Shear and (b) kinematic viscosity of the $Al_{100-x}Cu_x$ melt vs. wavenumber k at a temperature $T = 973$ K, a pressure $p = 1.0$ bar, and various atomic copper concentrations.

per atoms ($x \geq 40\%$), the kinematic viscosity is interpolated by a linear dependence $\nu(x) = ax + b$, where $a = 5.9 \times 10^{-9}$ m^2/(at % s) and $b = 3.34 \times 10^{-7}$ m^2/s. A deviation from the linear dependence is observed in the case of equilibrium melt at $x < 40\%$. An insignificant "shoulder" in the $\nu(x)$ dependence, which is also supported by the experimental results, is detected at a low copper concentration ($x < 20\%$). This shoulder is

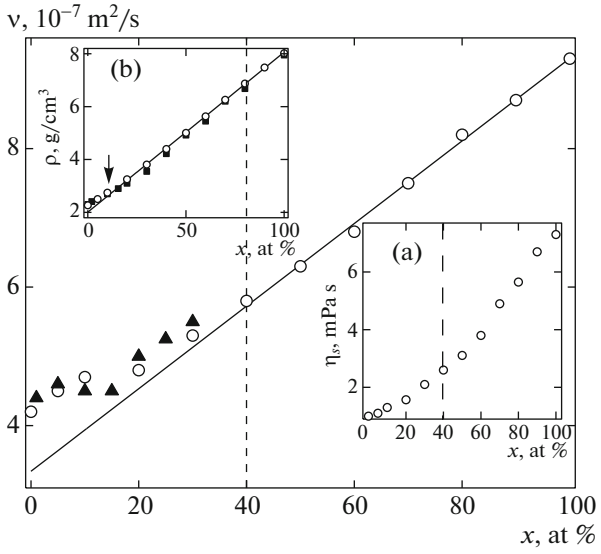

Fig. 9. Concentration dependence of the kinematic viscosity of the $Al_{100-x}Cu_x$ melt at $T = 973$ K: (○) results of atomic dynamics simulation and (▲) experimental data. Insets: (a) shear viscosity of the $Al_{100-x}Cu_x$ melt vs. the atomic copper concentration at $T = 973$ K and (b) concentration dependence of system density ρ ((○) simulation results, (■) experimental data at $T = 1020$ K [41, 42].

caused by the specific features in the concentration dependence of the density $\rho(x)$ (see inset (b) in Fig. 9). This specific feature of $\nu(x)$ manifests itself at the copper concentrations that are characteristic of the maximum velocity of longitudinal polarization sound (see Fig. 7).

5. CONCLUSIONS

A large-scale simulation of the atomic dynamics of the $Al_{100-x}Cu_x$ melt was performed at a temperature $T = 973$ K and various atomic copper concentrations (0–100%). When analyzing the equilibrium structural characteristics of the $Al_{100-x}Cu_x$ melt, we showed that the concentration dependence of the translational order parameter correctly predicts the transition from the state of equilibrium liquid into the state of supercooled melt at an atomic copper concentration $x = 40\%$.

The calculated spectral densities of the time correlation functions of the longitudinal $\tilde{C}_L(k,\omega)$ and transverse $\tilde{C}_T(k,\omega)$ currents for the supercooled $Al_{100-x}Cu_x$ melt at a temperature $T = 973$ K exhibit propagating collective excitations of longitudinal and transverse polarizations over a wide wavenumber range. A correlation was found between the structural features and the acoustic properties of the aluminum–copper system over the entire atomic copper concentration range under study. It was shown that the maximum sound velocity in the $v_L(x)$ concentration dependence takes place for the equilibrium melt ($x < 40\%$), whereas the supercooled $Al_{100-x}Cu_x$ melt saturated with copper atoms ($x \geqslant 40\%$) is characterized by the minimum sound velocity ($v_L \approx 3.94$ km/s). The character of the $v_L(x)$ dependence was found to correlate with the concentration dependence of parameter $S_m(x)$, whereas the velocity of transverse polarization sound $v_T(x)$ decreases from 2.74 to 1.79 km/s with increasing copper concentration.

Based on atomic dynamics simulation, we calculated the concentration dependences of the coefficients of shear $\eta_s(x)$ and kinematic $\nu(x)$ viscosities. As the copper concentration increases, the kinematic viscosity was found to increase from 4.2×10^{-7} to 9.3×10^{-7} m²/s. The total concentration dependence was found to be characterized by two modes. In the case of the supercooled melt saturated with copper atoms ($x \geq 40\%$), kinematic viscosity $\nu(x)$ is interpolated by a linear dependence, and a deviation from the linear dependence is observed in the case of equilibrium melt at $x < 40\%$. An insignificant shoulder in the $\nu(x)$ dependence, which can be caused by the specific features in the concentration dependence of the system density $\rho(x)$, was observed at low copper concentrations ($x < 20\%$).

ACKNOWLEDGMENTS

The large-scale molecular dynamics simulation was performed on the computational cluster of Kazan Federal University and on the supercomputer of the Interdepartmental Supercomputer Center of the Russian Academy of Sciences.

This work was supported in part by the Russian Foundation for Basic Research, project nos. 14-02-00335-a and 15-02-06288-a.

REFERENCES

1. N. H. March, *Liquid Metals: Concepts and Theory* (Cambridge Univ. Press, Cambridge, 1990).
2. R. Hultgren, *Selected Values of the Thermodynamic Properties of Binary Alloys* (Amer. Soc. Metals, Metals Park, Ohio, 1973).
3. A. T. Dinsdale and P. N. Quested, J. Mater. Sci. **39**, 7221 (2004).
4. *The 140th Committee of Japan Society for Promotion of Science: Handbook of Physico-Chemical Properties at High Temperature*, Ed. by Y. Kawai and Y. Shirai-shi (ISIJ, Tokyo, 1988).
5. R. M. Khusnutdinov and A. V. Mokshin, Bull. Russ. Acad. Sci.: Phys. **74**, 640 (2010).
6. Y. He, S. J. Poon, and G. J. Shiflet, Science **241**, 1640 (1988).
7. A. P. Tsai, A. Inoue, and T. Masumoto, J. Mater. Sci. Lett. **7**, 805 (1988).
8. V. V. Brazhkin, Phys. Usp. **49**, 719 (2006).
9. M. Sun and X. Bian, Mater. Lett. **56**, 620 (2002).

10. W. R. D. Jones and W. L. Bartlett, J. Inst. Metals **83**, 59 (1954).
11. K. I. Eretnov and A. P. Lyubimov, Izv. Vyssh. Uchebn. Zaved., Tsvet. Metall. **1**, 119 (1966).
12. M. Schick, J. Brillo, I. Egry, and B. Hallstedt, J. Mater. Sci. **47**, 8145 (2012).
13. N. Yu. Konstantinova, P. S. Popel', and D. A. Yagodin, High Temp. **47**, 336 (2009).
14. A. V. Mokshin, A. V. Chvanova, and R. M. Khusnutdinov, Theor. Math. Phys. **171**, 541 (2012).
15. V. T. Witusiewicz, U. Hecht, S. G. Fries, and S. Rex, J. Alloys Comp. **385**, 133 (2004).
16. C. W. Bale, P. Chartrand, S. A. Degterov, et al., CALPHAD **26**, 189 (2002). http://www.crct.polymtl.ca/fact/download.php
17. J. Cai and Y. Y. Ye, Phys. Rev. B **54**, 8398 (1996).
18. D. K. Belashchenko, Phys. Usp. **56**, 1176 (2013).
19. R. M. Khusnutdinoff, A. V. Mokshin, and I. I. Khadeev, J. Phys.: Conf. Ser. **394**, 012012 (2012).
20. A. L. Bel'tyukov and V. I. Lad'yanov, Instrum. Exp. Tech. **51**, 304 (2008).
21. O. Yu. Goncharov, N. V. Olyanina, A. L. Bel'tyukov, and V. I. Lad'yanov, Russ. J. Phys. Chem. A **89**, 857 (2015).
22. E. G. Shvidkovskii, *Some Questions of the Viscosity of Fused Metals* (Gostekhizdat, Moscow, 1955) [in Russian].
23. A. L. Bel'tyukov, S. G. Men'shikova, and V. I. Lad'yanov, High Temp. **53**, 491 (2015).
24. R. M. Khusnutdinov, A. V. Mokshin, and I. I. Khadeev, J. Surf. Invest.: X-ray, Synchrotron Neutron Tech. **8**, 84 (2014).
25. J. P. Hansen and I. R. McDonald, *Theory of Simple Liquids* (Academic, New York, 2006).
26. A. V. Mokshin, R. M. Yulmetyev, R. M. Khusnutdinov, and P. Hanggi, J. Exp. Theor. Phys. **103**, 841 (2006).
27. Y. Waseda, *The Structure of Non-Crystalline Materials: Liquids and Amorphous Solids* (McGraw-Hill, New York, 1980).
28. T. M. Truskett, S. Torquato, and P. G. Debenedetti, Phys. Rev. E **62**, 993 (2000).
29. R. M. Khusnutdinov, A. V. Mokshin, and R. M. Yulmetyev, J. Exp. Theor. Phys. **108**, 417 (2009).
30. W. Montfrooij and I. de Schepper, *Excitations in Simple Liquids, Liquid Metals and Superfluids* (Oxford Univ. Press, New York, 2010).
31. R. M. Khusnutdinov and A. V. Mokshin, JETP Lett. **100**, 39 (2014).
32. R. M. Khusnutdinov, A. V. Mokshin, and I. D. Takhaviev, Phys. Solid State **57**, 412 (2015).
33. A. V. Mokshin, R. M. Khusnutdinov, A. G. Novikov, N. M. Blagoveshchenskii, and A. V. Puchkov, J. Exp. Theor. Phys. **121**, 828 (2015).
34. D. Pines, *Elementary Excitations in Solids* (W. A. Benjamin, New York, 1963).
35. U. Balucani and M. Zoppi, *Dynamics of the Liquid State* (Clarendon, Oxford, 1994).
36. A. V. Mokshin, R. M. Yulmetyev, R. M. Khusnutdinoff, and P. Hänggi, J. Phys.: Condens. Matter **19**, 046209 (2007).
37. T. Gaskell, U. Balucani, M. Gori, and R. Vallauri, Phys. Scripta **35**, 37 (1987).
38. V. I. Lad'yanov, A. L. Bel'tyukov, S. G. Menshikova, and A. U. Korepanov, Phys. Chem. Liquids **52**, 46 (2014).
39. A. L. Bel'tyukov, S. G. Menshikova, and V. I. Lad'yanov, J. Non-Cryst. Solids **410**, 1 (2015).
40. W. E. Alley and B. J. Alder, Phys. Rev. A **27**, 3158 (1983).
41. J. Brillo, I. Egry, and J. Westphal, Int. J. Mater. Res. **99**, 162 (2008).
42. Y. Plevachuk, V. Sklyarchuk, A. Yakymovych, et al., Metal. Mater. Trans. A **39**, 3040 (2008).

Translated by K. Shakhlevich